Nationaal Lucht- en Ruimtevaartlaboratorium
National Aerospace Laboratory NLR

NLR-TP-2001-446

Computations of three-dimensional unsteady supersonic cavity flow to study the effect of different downstream geometries

B.I. Soemarwoto and J.C. Kok

Nationaal Lucht- en Ruimtevaartlaboratorium
National Aerospace Laboratory NLR

NLR-TP-2001-446

Computations of three-dimensional unsteady supersonic cavity flow to study the effect of different downstream geometries

B.I. Soemarwoto and J.C. Kok

This report is based on a presentation held at the AVT Symposium on Aging Mechanisms and Control Development in Computational Aero- and Hydro-Acoustics, Manchester, UK, 8-11 October 2001.

Division:	Fluid Dynamics
Issued:	November 2001
Classification of title:	Unclassified

Contents

(15 pages in total)

Computations of three-dimensional unsteady supersonic cavity flow to study the effect of different downstream geometries

B. I. Soemarwoto and J.C. Kok
National Aerospace Laboratory NLR
Anthony Fokkerweg 2, 1059 CM Amsterdam
soemarwt@nlr.nl, jkok@nlr.nl

for presentation at the AVT Symposium on Aging Mechanisms and Control, Development in Computational Aero- and Hydro-Acoustics, Manchester, UK, 8-11 October 2001

Abstract

Computations of three-dimensional unsteady supersonic cavity flow are performed for a free-stream Mach number of 1.2. Two cavity geometries are considered: (i) a simple rectangular cavity of length-to-depth (L/D) and length-to-width (L/W) ratios of 4.5, and (ii) a cavity with a 45° ramp attached to the downstream wall of the simple rectangular cavity. Two flow models for computing the cavity flowfield are assessed: (a) the Reynolds-Averaged Navier-Stokes (RANS) equations with a k-ω turbulence model for the whole flowfield, and (b) a combination of an inviscid flow model using the Euler equations for the domain outside the boundary layer and the RANS model for the boundary layer. The structures of the flowfields resulting from the different models are observed. The effect of the different downstream geometries is assessed.

INTRODUCTION

The aeroacoustic environment arising from the three-dimensional supersonic flowfield around cavities is closely related with aeroacoustic loads on aircraft components, for example when weapon bays are open at supersonic speeds. The aeroacoustic environment can be separated into the broad-band noise representing pressure fluctuations typically produced by the turbulence, and the narrow-band discrete tones due to resonance involving finite-amplitude self-sustained pressure oscillations inside the cavity. Cavity geometries are characterized by the length-to-depth (L/D) ratio that determines the flowfields to be either closed, open or transitional (intermediate). Closed cavity flowfields are typically associated with shallow cavities ($L/D > 13$) producing broad-band noise. In this type of flow, the shear layer hits the bottom of the cavity, forming two recirculating regions inside the cavity under the shear layer. Open cavity flowfields are typically associated with deep cavities ($L/D < 10$) producing broad-band noise accompanied by distinct narrow-band discrete tones. This type of flow consists of internal and external regions separated by the shear layer spanning along the cavity opening, where the internal region contains a large recirculating flow. An intermediate value of $10 < L/D < 13$ is associated with transitional cavity flowfields.

Numerous prior experimental [1]-[4] and numerical [5]-[15] investigations have been performed. For example, methods based on the Euler equations [5],[15], laminar Navier-Stokes equations [13], Reynolds-Averaged Navier-Stokes (RANS) equations with algebraic [6],[7],[10] and two-equation [8],[9],[12] turbulence models, LES [11],[15], and DNS [14] have been applied. Unfortunately, the results from this large variation of flow models do not seem to lead to a definite conclusion as to which flow modelling is most suitable for simulating three-dimensional cavity flowfields. Although LES and DNS methods undoubtly have the highest potentials for capturing the complete physics, they require prohibitively high computational resources, especially when three-dimensional configurations and high Reynolds numbers are involved. For a routine use, such as for evaluating effects of different cavity geometries, RANS and Euler methods should be assessed for their applicability.

In the present investigation, an open cavity flowfield is considered with $L/D = 4.5$. Time-accurate computations of the three-dimensional supersonic flow over a cavity at a Mach number of $M = 1.2$ and a Reynolds number of $Re = 4.5 \cdot 10^6$ are performed using the NLR CFD system ENFLOW [16],[18]. This CFD system employs multi-block structured grids to simulate three-dimensional flows, where a different flow model may be defined in each block. Two approaches for modelling the cavity flowfield are taken. The first approach is to apply the RANS equations with a k-ω turbulence model for the whole flow domain of the

cavity configuration. In the second approach, an inviscid flow model using the Euler equations is applied in combination with the RANS equations and the k-ω turbulence model for the boundary layer regions over the solid surfaces including those of the cavity walls.

Shear layer instabilities have been found to play an important role in the formation of the self-sustained oscillations, while alternating impingements of the shear layer on the downstream edge of the wall appear to influence the amplitude of the oscillations. The shear layer impingements can be altered through modifying the geometry of the downstream edge. The frequency spectra of the sound pressure level, and in turn the aeroacoustic loads, can therefore be influenced by the geometry of the downstream edge.

The flowfields around a simple rectangular cavity and around a cavity of the same L/D ratio with a 45° solid ramp attached on the downstream edge will be computed. Results from the two different flow models will be discussed, and effects of the downstream edge geometries will be identified.

MODELLING OF THE FLOW

The two cavity geometries, a simple rectangular cavity and a cavity with a 45° ramp shown in Figure 2, are adopted from the WICS model [2]. The flow is assumed symmetrical with respect to the X-Z plane at the centreline of the cavity. The geometry is represented by a half model consisting of two parts: the cavity and a flat plate surrounding the cavity opening. The solid surfaces consist of the flat plate and the cavity walls.

Figure 1 gives an impression of the block topology used for both cavity geometries. The flow domain is decomposed into 13 blocks. A layer of blocks (blue) is constructed over the solid surfaces to represent the boundary layer regions. This layer is connected to the far-field boundaries by another layer of larger blocks (green). A block (red) is introduced upstream of the flat plate where the flow is treated as inviscid. This block allows the flow to enter the domain as a uniform flow, and to stagnate at the leading edge of the flat plate where the boundary layer starts. Downstream of the flat plate, another block (yellow) with an inviscid flow is placed connecting the cavity flowfield with the far-field outflow boundary.

Within each block a structured grid is generated. Inside the blocks associated with the boundary layer, a finer distribution of the grid points is applied towards the solid surface in order to adequately resolve the turbulent boundary layer. Outside these blocks, the computational grids are constructed to be approximately uniform and isotropic. The computational grids on the solid surfaces and those on the symmetry planes are shown in Figure 2 and Figure 3, respectively. The domain inside the cavity is represented by 262144 grid cells, of which 192x32x16 grid cells fill the domain inside the cavity but outside the boundary layers. The whole flow domain contains a total of 655360 grid cells.

Adiabatic no-slip boundary conditions are applied for all solid surfaces. Symmetry conditions are enforced on the X-Z plane at $Y = 0$ coinciding with the cavity centreline. On the horizontal surface upstream of the flat plate, a slip (zero normal velocity) condition is applied. This surface ensures that the flow enters the domain as a uniform flow and the boundary layer starts at the leading edge of the flat plate. Laminar boundary layers are assumed to cover up to 5% of the length measured from the flat plate leading edge to the cavity, downstream of which the boundary layers are assumed to be fully turbulent. On the side boundary, opposite to the symmetry plane, flow variables are enforced to have a zero gradient. Characteristics-based boundary conditions are applied on the far-field boundaries.

Two approaches in modelling the flow are considered. In the first approach, all blocks (green and blue) inside and around the cavity contain a viscous, turbulent flow governed by the RANS equations with a k-ω turbulence model. In the second approach, an inviscid flow governed by the Euler equations is applied to the green blocks, while the same RANS model is used inside the boundary layer blocks (blue).

The k-ω turbulence model [17] used in the computations employs a new set of diffusion coefficients to resolve the free-stream dependency problem of the original Wilcox k-ω model. Also, in the turbulence model a τ formulation for ω is implemented [18], where $\tau = 1/\omega$ is treated as a dependent variable instead of ω. This formulation avoids the problem of the singular behaviour of ω at solid walls.

For any instant of time, the cavity flowfield contains vortical flow structures. It is well known that for vortical flows the standard k-ω turbulence model is too diffusive to capture flow details near vortex cores. To cope with this problem, a parameter representing the ratio between the magnitude of the strain-rate tensor and the magnitude of vorticity is introduced to detect vortex cores. This parameter is used to increase the production term of the ω-equation, giving an effect of increasing the dissipation of the turbulence kinetic energy and of the eddy viscosity. This modification for vortical flow computations, which has been successfully applied to vortex dominated flows around delta wings [19], is also used in the present investigation.

The continuous equations are discretized in space using a cell-centred finite-volume scheme. Jameson-type second-order and fourth-order diffusion terms are introduced to capture shock waves and to prevent odd-even decoupling, respectively. Matrix coefficients are used for the artificial diffusion terms. These coefficients have shown to be less diffusive than the standard scalar coefficients. The so-called dual-time stepping scheme is applied for the time integration of the unsteady equations which is second-order accurate.

RESULTS AND DISCUSSION

Simple rectangular cavity

For the simple rectangular cavity, computations are performed for a Mach number $M = 1.2$ and a Reynolds number $Re = 4.5 \cdot 10^6$. Rossiter's formula [1] is considered for estimating the cavity resonance frequencies:

$$f = \frac{V_\infty}{L} \frac{m - \gamma}{\frac{1}{\Phi_d} + \frac{a_\infty}{a_t} M_\infty}, \qquad \textbf{(1)}$$

where $\gamma = 0.28$ and $\Phi_d = 0.57$ are used for $L/H = 4.5$. Index $m = 1,2,\ldots$ refers to the resonance mode, while a_∞ and a_t are the speeds of sound based on the free-stream total temperature and free-stream static temperature, respectively. The second resonance mode typically has a distinctive peak in the frequency spectrum, which is estimated by the above equation to be equal to 502 Hz. A sampling rate of about 10000 samples per second is selected in order to adequately resolve the second mode frequency by about 20 data points. This sampling rate defines the time step:

$$\Delta t = 0.0812\, t_c, \qquad \textbf{(2)}$$

where the characteristic time t_c is the time required by the flow to traverse the length of the cavity. The data from the experiment [1] provides

$$t_c = \frac{L}{V_\infty} = 1.2305 \cdot 10^{-3} \text{ s}. \qquad \textbf{(3)}$$

After the starting transients have decayed, a sample size of $N = 1024$ time steps is produced from the time-accurate unsteady flow computations. The unsteady static pressure is observed at a grid point corresponding to the experimental pressure transducer K16 which is located on the bottom of the cavity at a distance of $0.015L$ from the aft wall.

Figure 4 presents the unsteady static pressure fluctuations and the frequency spectra. The Sound Pressure Level (SPL) in the frequency spectra is defined as:

$$\text{SPL} = 180 + 20 \log\left(\frac{p}{p_{\text{ref}}} \right) \text{dB}, \qquad \textbf{(4)}$$

where $p_{\text{ref}} = 2.90075$ psi is the standard reference pressure.

The RANS model results in almost purely periodical fluctuations, in contrast with those obtained from the Euler with boundary layer model. The maximum amplitudes of the RANS model are significantly lower than those of the other model. The RANS model produces a distinct resonance at 518 Hz (peak B). This frequency matches the second mode at 518 Hz measured in the experiment. There is also a close agreement in the magnitude which is within the range of 2 dB. It is not clear whether Peak A at 205 Hz corresponds to the experimental value of the first mode at 225 Hz, because its magnitude is much lower (20 dB less) than that of the experimental value. Peaks C and D are precisely the multiples of 518 Hz (1037 Hz and 1555 Hz, respectively), and therefore should not be associated with the higher modes.

The Euler with boundary layer model produces two distinct peaks (numbered 1 and 2) at 215 Hz and 509 Hz. These frequencies are reasonably close to the experimental values, 225 Hz and 518 Hz, of the first and second modes. The third and higher modes occur in the experiment at 830 Hz and 1025 Hz, respectively. Peaks 3 and 4 appear at 812 Hz and 1008 Hz, though not distinctively, and have amplitudes that are in the

range of 2 dB from the experimental values. The amplitude of the first (second) peak is within 2 dB (5 dB) difference from that of the first (second) mode's amplitude of the experiment.

Figures 5 and 6 present the instantaneous flow patterns produced by the RANS model which belong to a cycle between two consecutive minimum values of the static pressure at the grid point observed. The total pressure loss contours in Figure 5 show wave-like oscillating shear layers associated with vortices travelling inside the cavity. The cycle appears to consist of the following sequence: (1) an upward deflection of the shear layer that leads to a fluid spill leaving the cavity, while a vortex has been formed downstream of the leading edge, (2-3) as the vortex moves downstream and gets stronger, the shear layer moves downward and its end impinges on the edge of the aft wall, (4-5) a compression wave (Figure 6) is formed in the aft wall region, (6) the downward movement of the shear layer induces fluid to enter the cavity and the pressure at the wall reaches a maximum, (7) the shear layer moves upward, (8-9) the vortex approaches the aft wall region while a new vortex is being formed near the leading edge, and (10) the process repeats itself. Figures 7 and 8 present the results obtained using the Euler with boundary layer model. Although the above sequence can still be identified, non-periodic oscillations are clearly indicated, in agreement with a larger number of frequency components resolved. The Euler boundary layer model results also show a more complex flow with eddies.

The overall sound pressure levels (OASPL) along the centreline of the cavity are also compared, where

$$\mathrm{OASPL} = 180 + 20\log\left(\frac{p_{\mathrm{rms}}}{p_{\mathrm{ref}}}\right)\mathrm{dB}\,, \qquad \textbf{(5)}$$

with the root-mean-square of the static pressure given by

$$p_{\mathrm{rms}} = \sqrt{\frac{1}{N}\sum\left(p_{\mathrm{ave}} - p\right)^2}\,. \qquad \textbf{(6)}$$

Figure 9 shows a same tendency produced by both flow models. The experimental values are obtained from the data presented in Ref. [7]. The full RANS model agrees well with the experiment, except in locations around the cavity mid-point. More discrepancies are observed for the results of the Euler with boundary layer model, especially in the downstream half of the cavity.

Cavity with ramp

The same computational procedure, with the same sampling rate of about 10000 per second, is also used for the cavity with ramp. The modification of the trailing edge geometry for this case shows to have a large impact on the cavity flowfield. The RANS model resulted in a steady flow, where the shear layer completely divided the flow into two domains inside and outside of the cavity.

The effect of the trailing edge geometry on the unsteady cavity flowfield can still be observed from the computations using the Euler with boundary layer model. Figure 10 shows the pressure fluctuations and the corresponding frequency spectra. The amplitudes of the pressure fluctuations are significantly smaller than those of the simple rectangular cavity (Figure 4). This indicates that the compression waves become much weaker by the ramp effects. The total pressure loss contours in Figure 11 show completely different flow patterns from those of the simple rectangular cavity, especially in the way the shear layer impinges on the aft wall as shown in pictures 2-5. Also, it can be observed in pictures 7-9 of Figure 12 that the propagation of the compression waves is partly deflected following the orientation of the ramp. The first and second resonance modes are increased by about 30 Hz and 38 Hz, respectively. A shorter effective distance between the upstream and downstream walls may be responsible for this increase in frequency. The amplitude of the first mode is decreased by about 5 dB, while that of the second mode is only slightly decreased. The higher modes are less identifiable, and possibly have significantly lower amplitudes.

The effect of the trailing geometries on the OASPL can be observed in Figure 13. The ramp has an effect of reducing the sound pressure level along the cavity centreline, except in a small region near the beginning of the ramp where the sound pressure level is slightly increased. Larger reductions are observed on the upstream wall and in the upstream part of the cavity.

CONCLUSIONS

Three-dimensional computations of supersonic flow around two cavities of L/D = 4.5 with different trailing edge geometries have been performed. Two flow models have been considered for the computations.

For the simple rectangular cavity, using the RANS equations with the k-ω turbulence model, we have been able to capture the frequency and magnitude of the second resonance mode, which agrees quite well with the measured values. Using the Euler model, in combination with modelling of the boundary layers using the RANS equations and the k-ω turbulence model, we have been able to capture the frequencies and amplitudes of the first four modes in reasonable agreement with the experimental values. With regard to the overall sound pressure level (OASPL) along the centreline of the cavity, the RANS model has been shown to produce a closer agreement with the experimental values, whereas the Euler with boundary layer model shows overpredictions in particular in locations downstream the cavity mid-point.

For the cavity with 45° ramp at the trailing edge, the RANS with k-ω model seems to be too dissipative to produce a self-sustained oscillation. The effect of the ramp has been assessed using the results from the Euler with boundary layer model. The ramp evidently reduces the amplitude of the pressure fluctuations. It is observed that the resonance modes have been increased slightly, while their amplitudes have been reduced.

The results clearly indicate that the RANS model is applicable only to limited cases of unsteady cavity flowfields. There seems to be a threshold, which is related to the physics of the unsteadiness, that separates unsteady solutions from steady solutions of the RANS equations. When an unsteady solution is obtained, however, the RANS model gives an accurate prediction of the resolved modes in terms of frequencies, amplitudes and OASPL. The Euler model in combination with RANS model for the boundary layer shows to be applicable to a large class of cavity flowfields, but it produces less accuracies especially in terms of OASPL. Finally, the best perpective for both an accurate simulation and a large class of cavity flowfields, at feasible computational costs, may be given by a hybrid LES model (replacing the Euler model) in combination with the RANS model for the boundary layer.

REFERENCES

[1] R.C. Bauer and R.E. Dix. *Engineering Model of Unsteady Flow in a Cavity*. AEDC-TR-91-17, 1991.
[2] R.E. Dix. Cavity aeroacoustics. Calspan Corporation/AEDC Operations.
[3] Kung-Ming Chung. A study of transonic rectangular cavity of varying dimensions. *AIAA Paper 99-1909*, 1999.
[4] M.A. Kegerise and E.F. Spina. An experimental investigation of flow-induced cavity oscillations. *AIAA Paper 99-3705*, 1999.
[5] C.J. Borland. Numerical prediction of the unsteady flowfield in an open cavity. *AIAA Paper 77-673*, 1977.
[6] D.P. Rizzetta. Numerical simulation of supersonic flow over a three-dimensional cavity. *AIAA Journal*, 26(7), 1988.
[7] N.E. Suhs. Unsteady flow computations for a three-dimensional cavity with and without an acoustic suppression device. *AIAA Paper 93-3402*, 1993.
[8] S.H. Shih, A. Hamed, and J.J. Yeuan. Unsteady supersonic cavity flow simulations using coupled k-ε and Navier-Stokes equations. *AIAA Journal*, 32(10), 1994.
[9] X. Zhang. Compressible cavity flow oscillation due to shear layer instabilities and pressure feedback. *AIAA Journal*, 33(8):1404--1411, 1995.
[10] C.J. Tam, P.D. Orkwis, and P.J. Disimile. Algebraic turbulence model simulations of supersonic open-cavity flow physics. *AIAA Journal*, 34(11):2255--2260, 1996.
[11] N. Sinha, S.M. Dash, and N. Chidambaram. A perspective on the simulation of cavity aeroacoustics. *AIAA Paper 98-0286*, 1998.
[12] X. Zhang, A. Rona, and J.A. Edwards. The effect of trailing edge geometry on cavity flow oscillation driven by a supersonic shear layer. *The aeronautical journal*, pages 129--136, March 1998.
[13] P.D. Orkwis, B. Sekar, S. Chakravarthy, and O. Peroomian. Comparison of three Navier-Stokes equation solvers for supersonic open cavity simulations. *AIAA Journal*, 36(5), 1998.
[14] T. Colonius, A.J. Basu, and C.W. Rowley. Numerical investigation of the flow past a cavity. *AIAA Paper 99-1912*, 1999.

[15] B.R. Smith, J.K. Jordan, E.E. Bender, S.N. Rizk, and L.L. Shaw. Computational simulation of active control of cavity acoustics. *AIAA Paper 2000-1927*, 2000.

[16] J.W. Boerstoel, A. Kassies, J.C. Kok, and S.P. Spekreijse. *ENFLOW, A full-functionality system of CFD codes for industrial Euler/Navier-Stokes Flow Computations*. NLR TP 96286 (presented at the 2nd Int. Symp. on Aeron. Science and Tech., Jakarta, 1996).

[17] J.C. Kok. Resolving the dependence on freestream values for the k-ω turbulence model. *AIAA Journal,* 38(7), pp. 1292–1294, 2000.

[18] J.C. Kok and S.P. Spekreijse. *Efficient and accurate implementation of the k-ω turbulence model in the NLR multi-block Navier-Stokes system*. NLR TP-2000-144 (presented at ECCOMAS 2000, Barcelona, Spain, 11-14 September, 2000).

[19] F.J. Brandsma, J.C. Kok, H.S. Dol, A. Elsenaar. *Leading edge vortex flow computations and comparison with DNW-HST wind tunnel data.* RTO/AVT Vortex Flow Symposium, Norway, 2001.

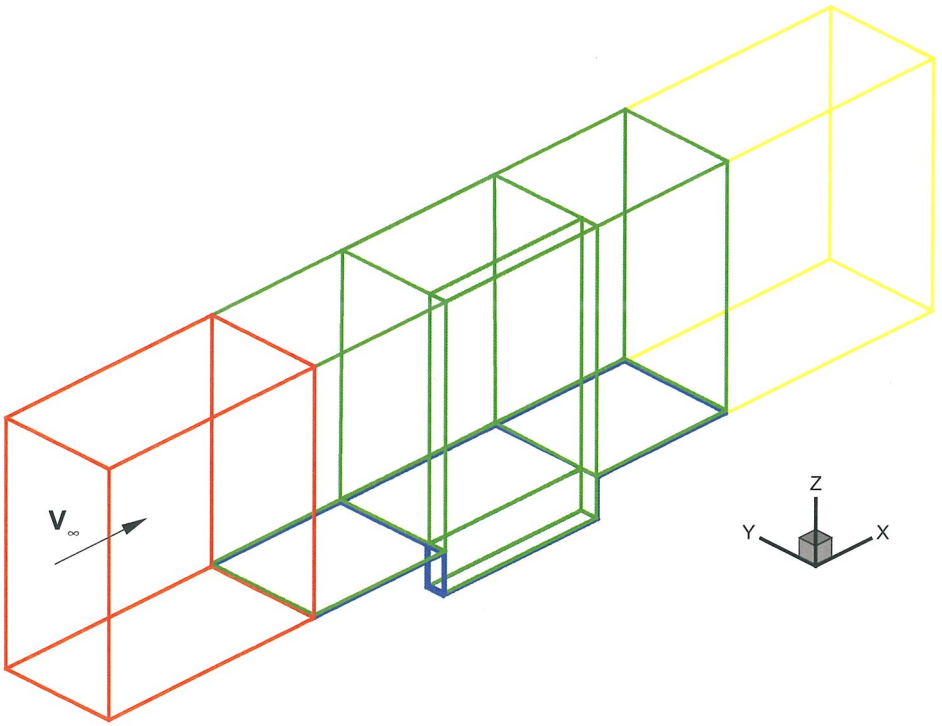

Figure 1 Flow domain modelling of the cavity flowfield.

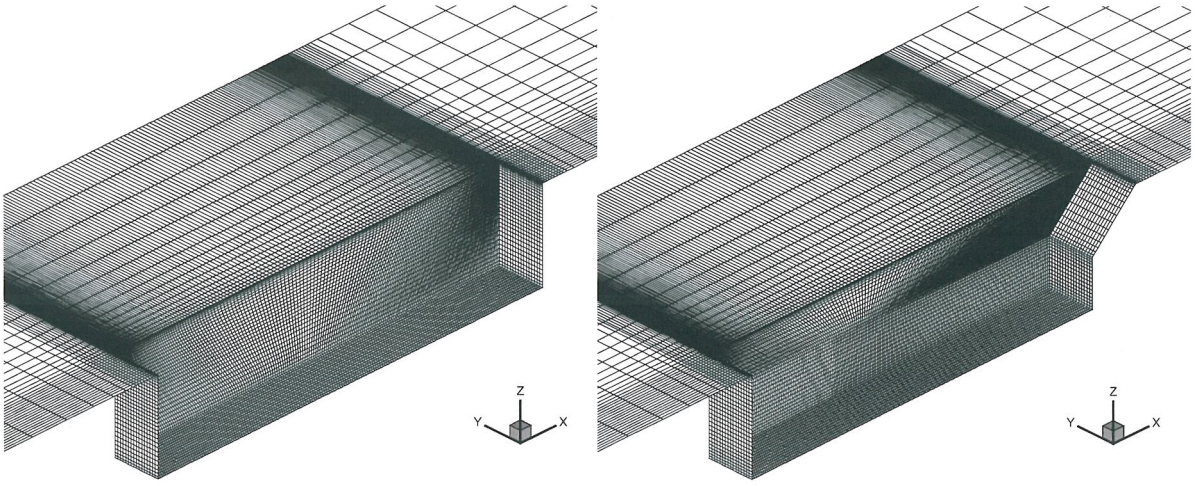

a) Simple rectangular cavity b) Cavity with ramp

Figure 2 Computational grids on the solid surfaces.

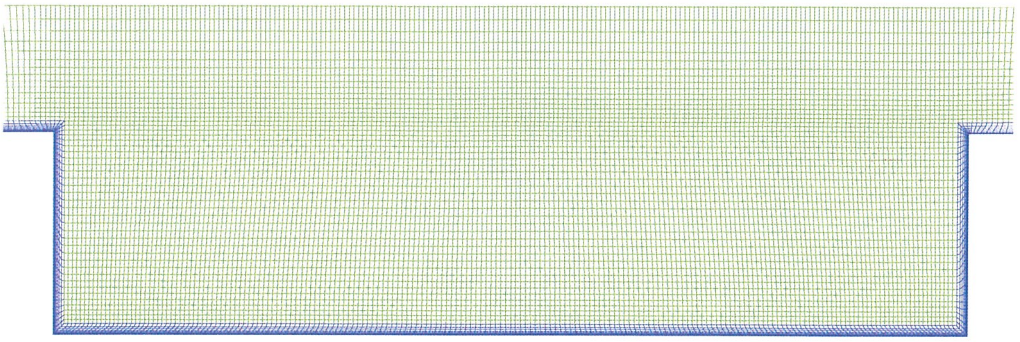

a) Simple rectangular cavity

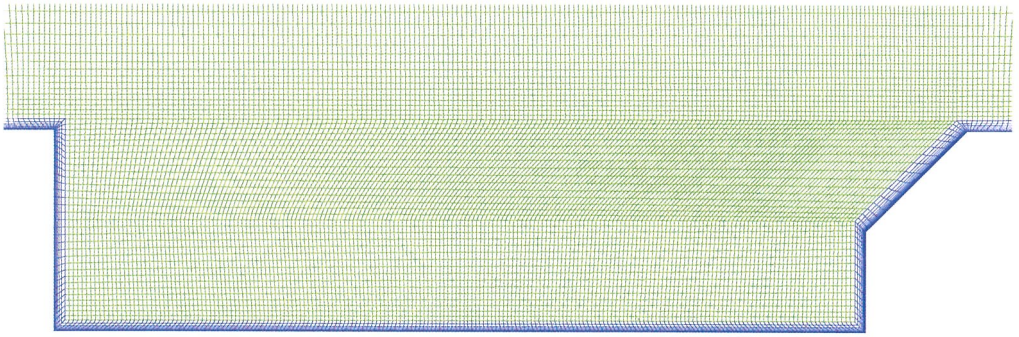

b) Cavity with ramp

Figure 3 Computational grids on the symmetry planes.

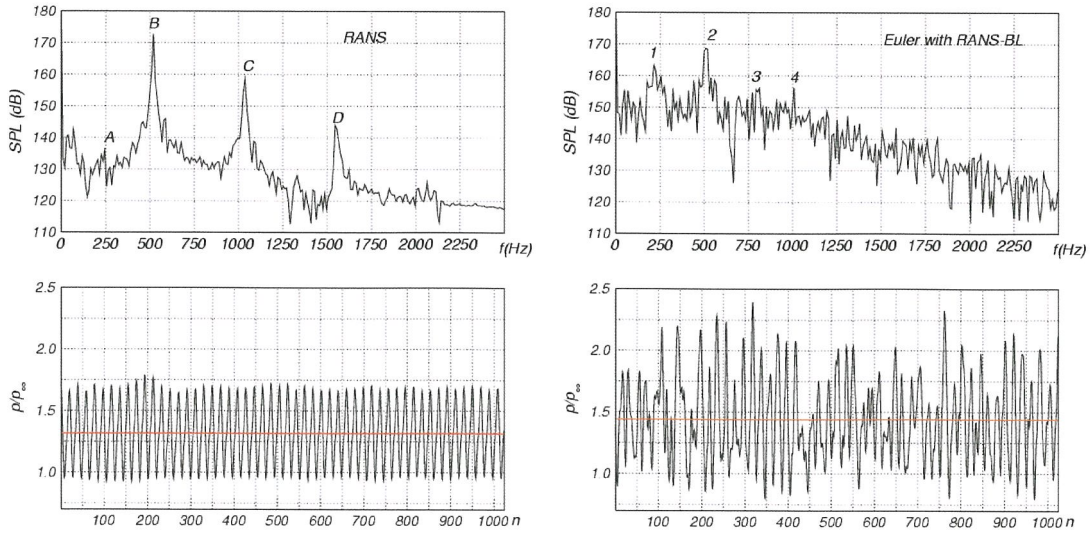

a) RANS b) Euler and RANS-BL

Figure 4 Unsteady pressure fluctuations and frequency spectra of the simple rectangular cavity flowfield.

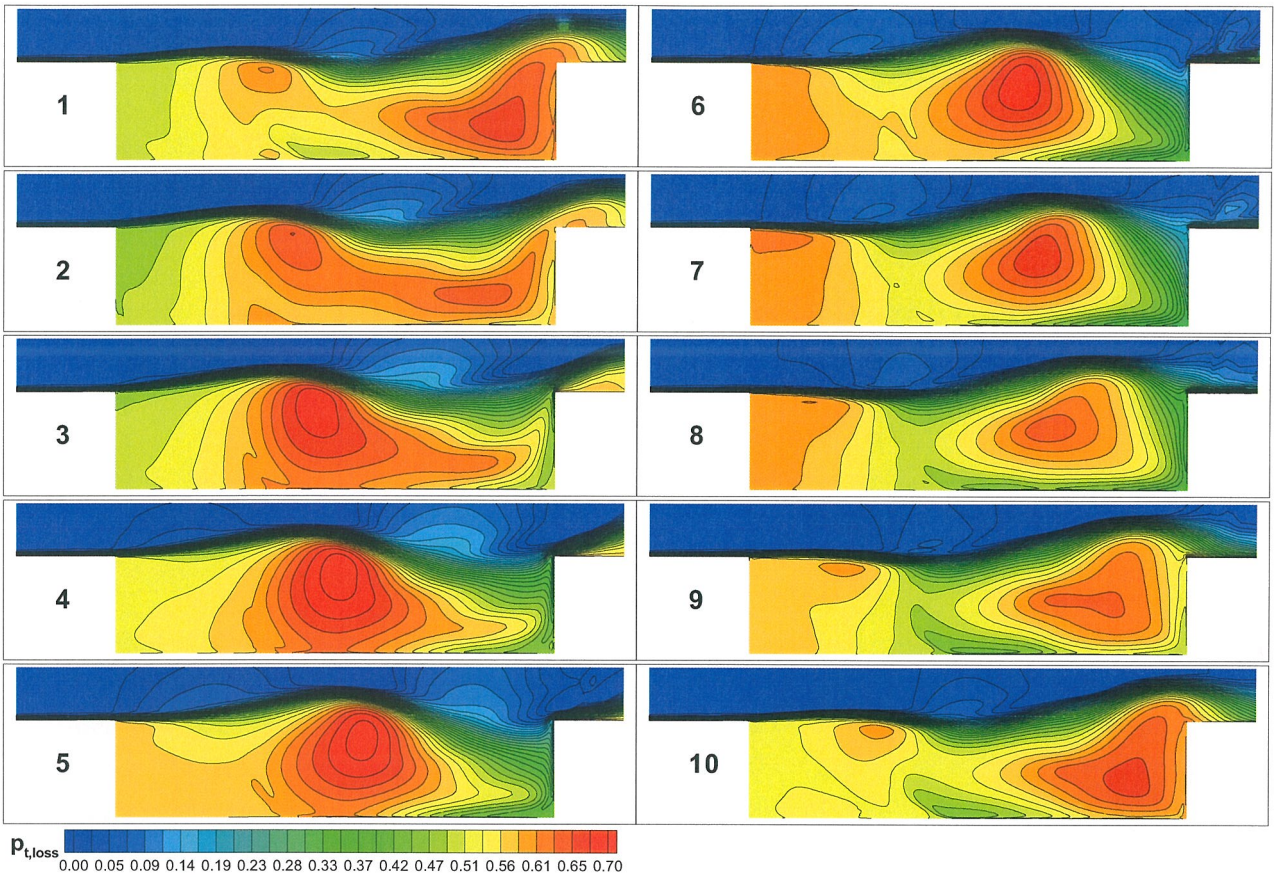

Figure 5 Instantaneous total pressure loss contours produced by the RANS model.

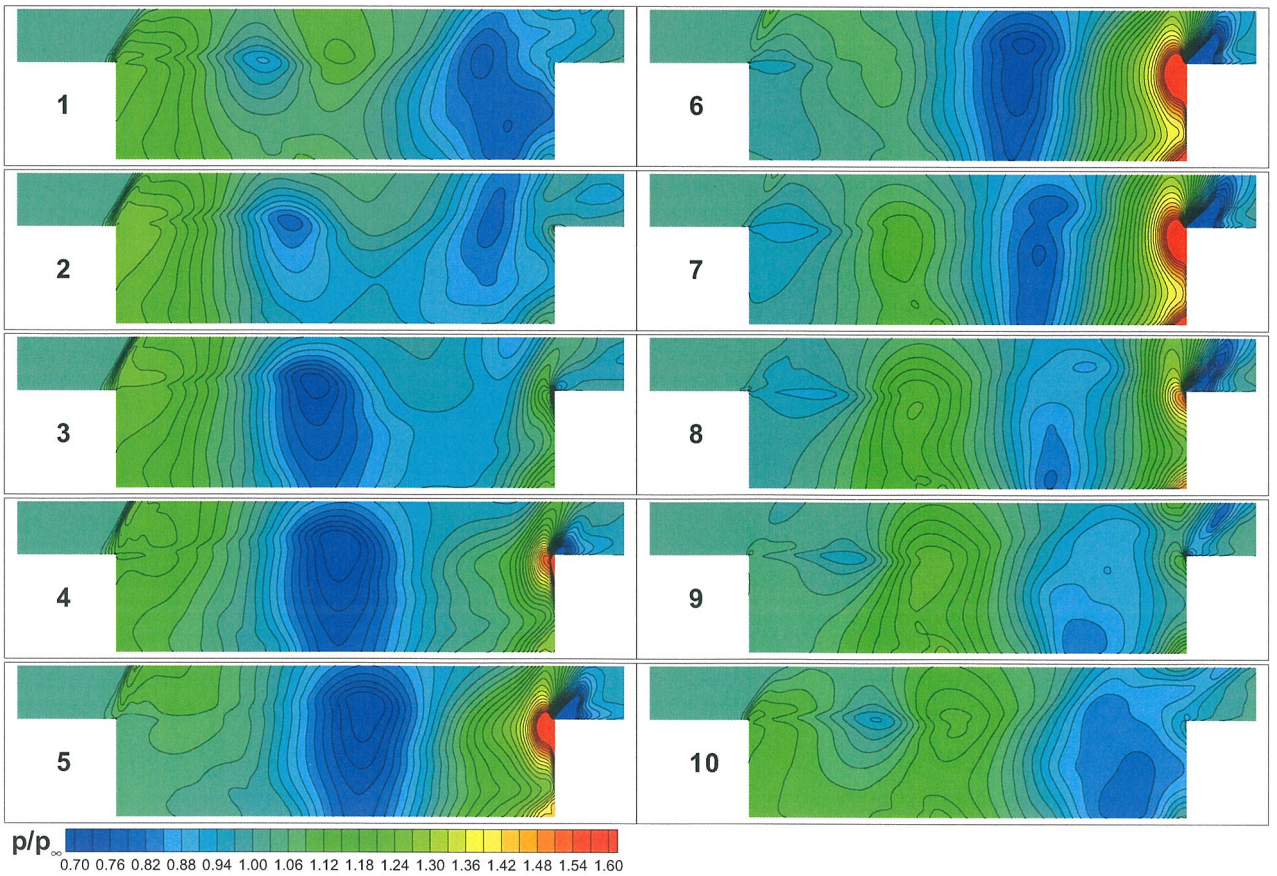

Figure 6 Instantaneous static pressure contours produced by the RANS model.

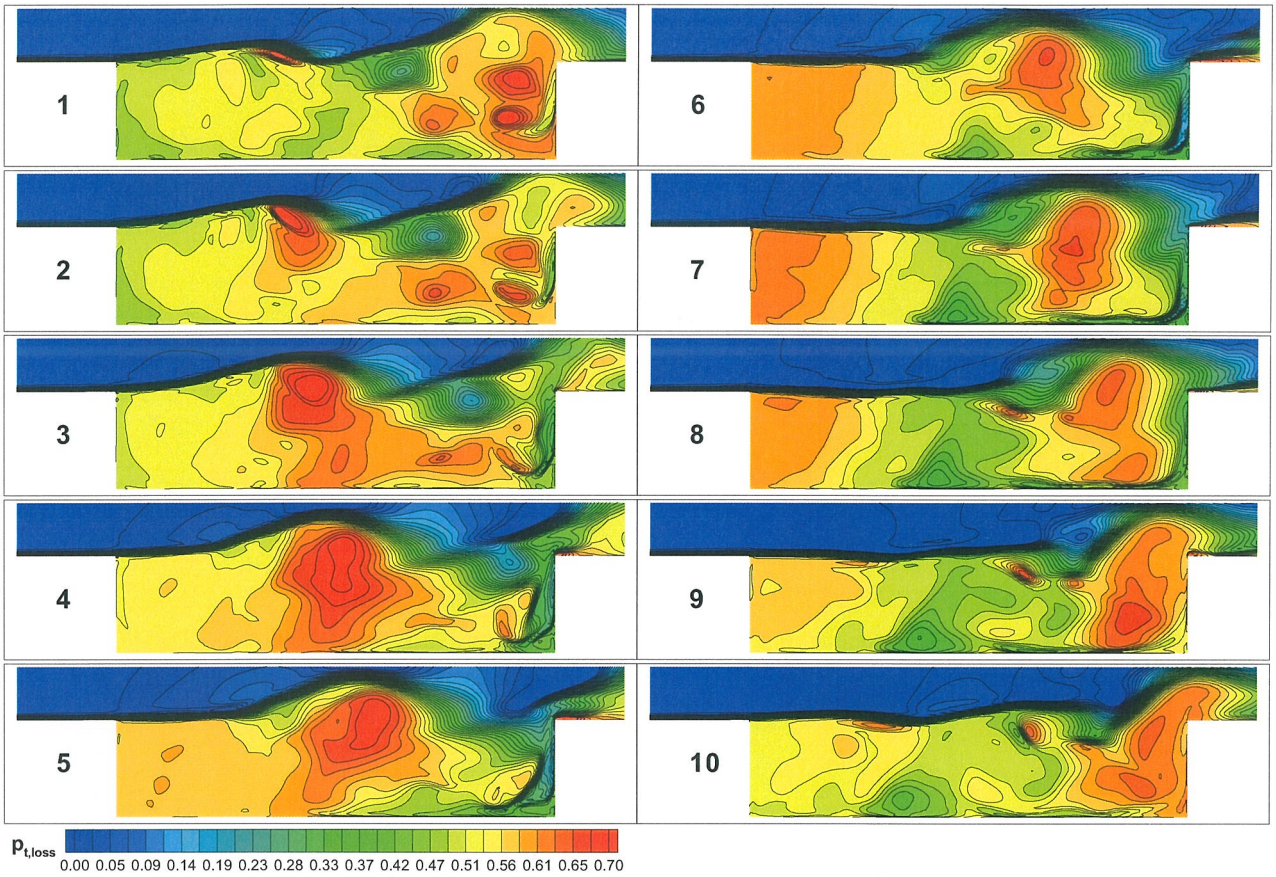

Figure 7 Instantaneous total pressure loss contours produced by the Euler with boundary layer model.

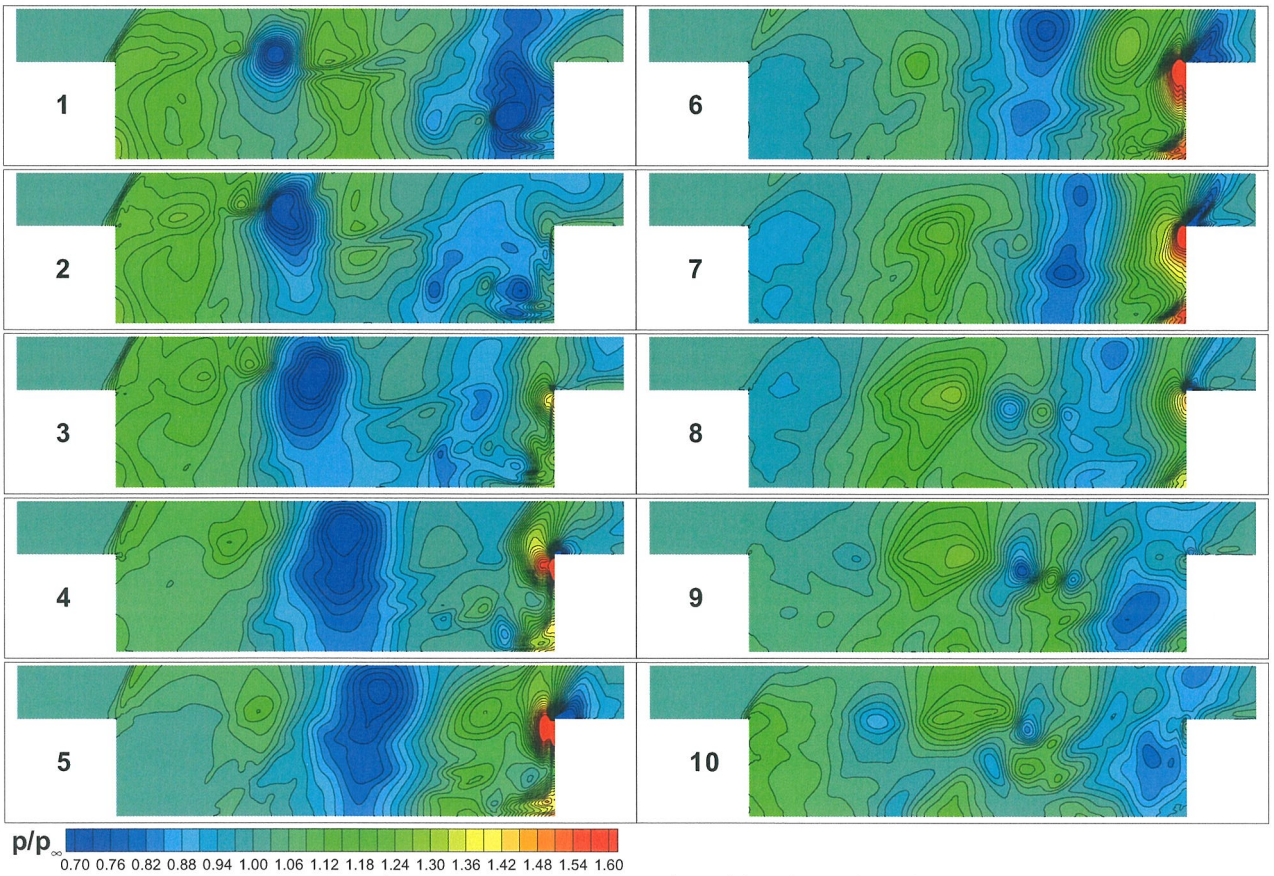

Figure 8 Instantaneous static pressure contours produced by the Euler with boundary layer model.

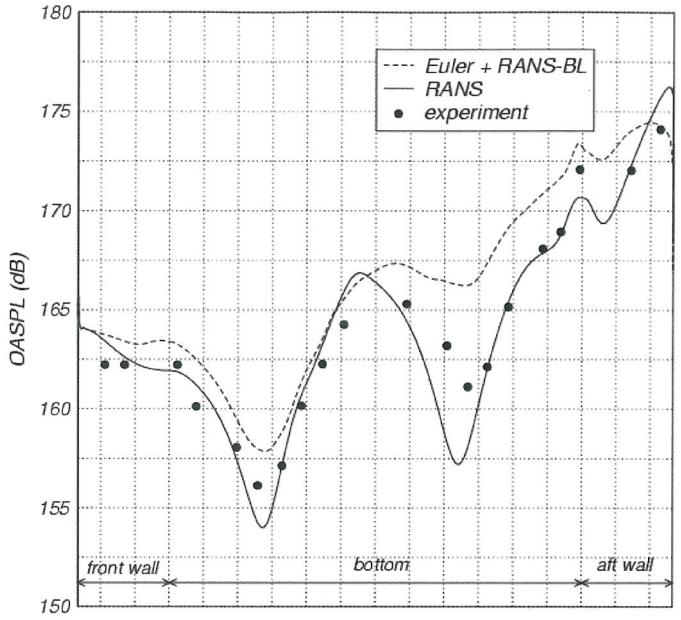

Figure 9 Overall sound pressure level (OASPL) along the centreline of the simple rectangular cavity (the experimental values are obtained from the data presented in Ref. [7]).

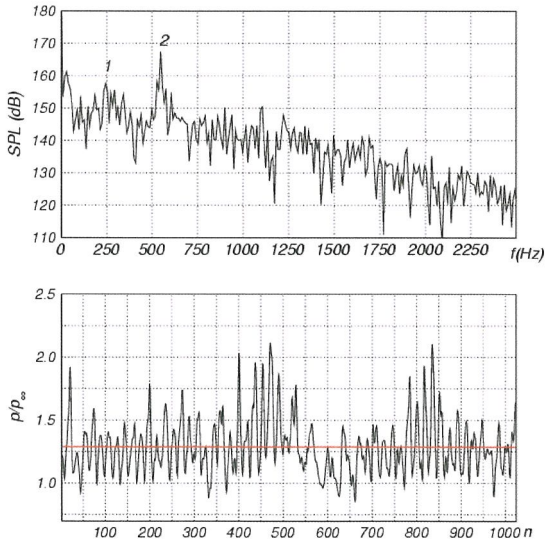

Figure 10 Unsteady pressure fluctuations and frequency spectra of the cavity with ramp.

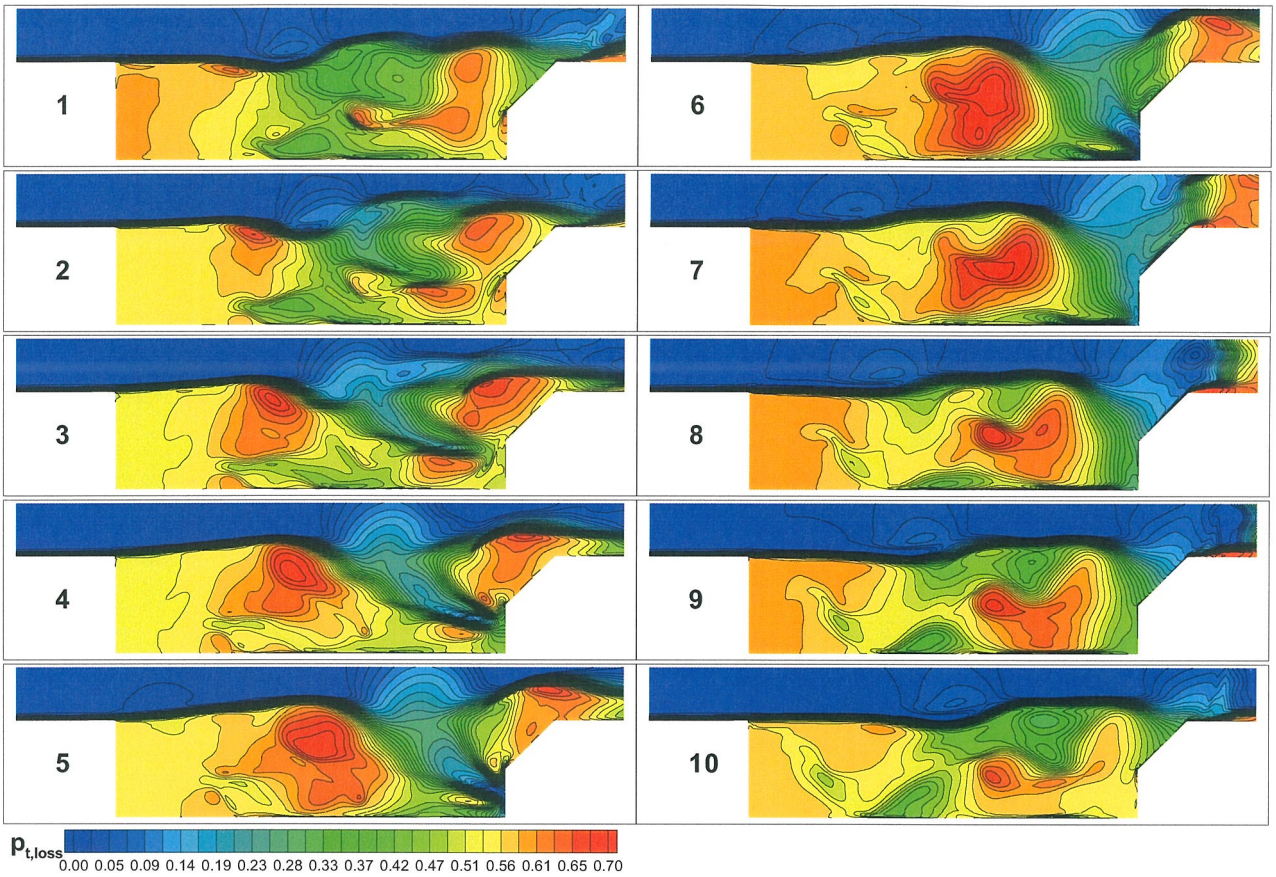

Figure 11 Instantaneous total pressure loss contours produced by the Euler with boundary layer model.

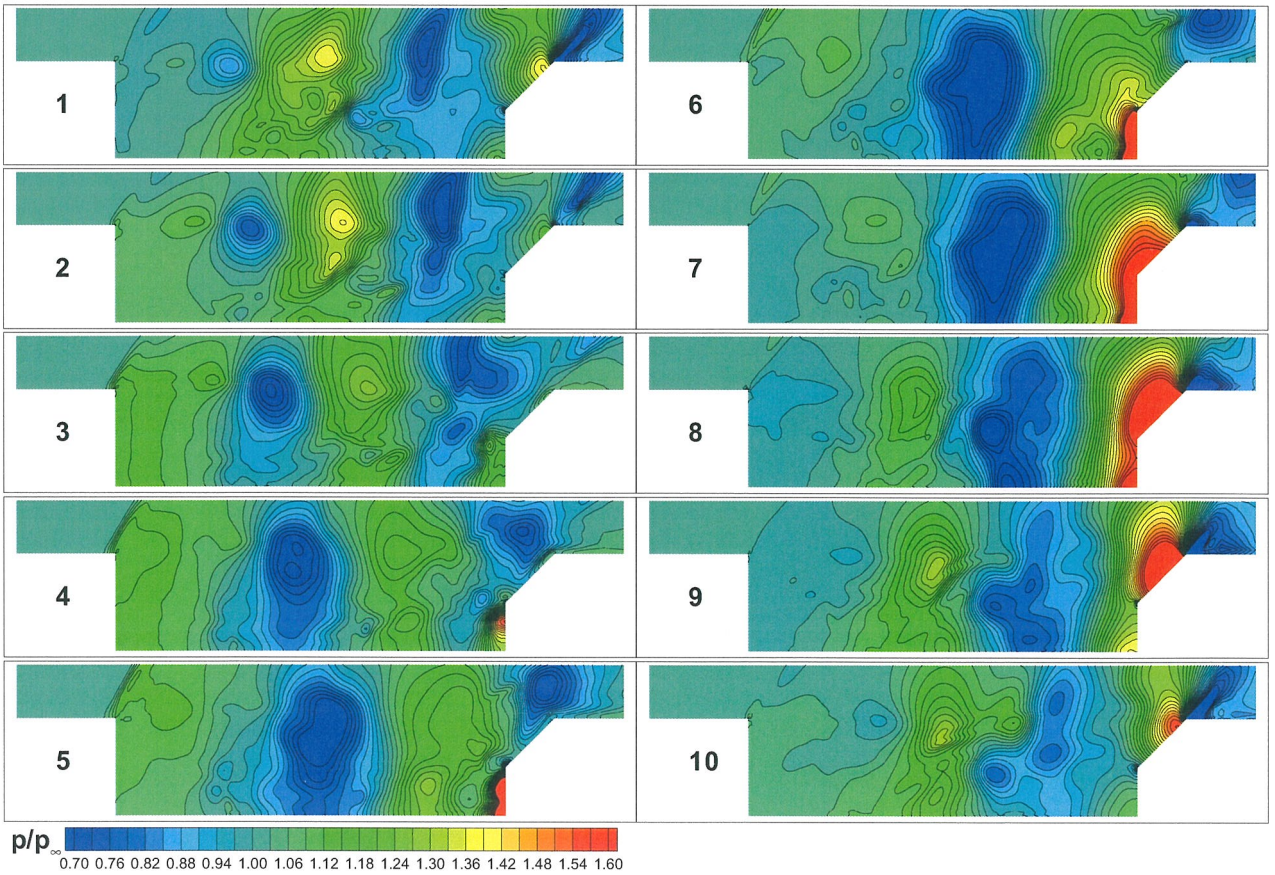

Figure 12 Instantaneous static pressure contours produced by the Euler with boundary layer model.

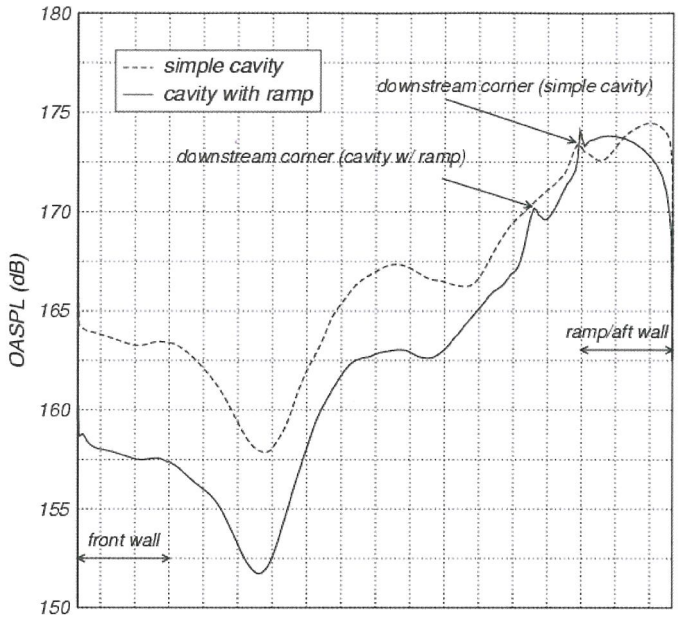

Figure 13 Effect of the trailing edge geometries to the overall sound pressure level.